NPS-MAE-22-003

NAVAL POSTGRADUATE SCHOOL

MONTEREY, CALIFORNIA

USING ADDITIVE PROCESSING TO HARNESS AND IMPLEMENT GRAPHENE TECHNOLOGY FOR WEAR AND CORROSION PROTECTION

by

Prof. Andy Nieto and Prof. Troy Ansell

September 2022

Prepared for: N9 - Warfare Systems. This research is supported by funding from the Naval Postgraduate School, Naval Research Program (PE 0605853N/2098).
NRP Project ID: NRP-22-N275-A.

THIS PAGE INTENTIONALLY LEFT BLANK

REPORT DOCUMENTATION PAGE

PLEASE DO NOT RETURN YOUR FORM TO THE ABOVE ORGANIZATION.

1. REPORT DATE	2. REPORT TYPE	3. DATES COVERED	
		START DATE	END DATE
10/18/2022	Technical Report	10/24/2021	10/22/2022

4. TITLE AND SUBTITLE

Using Additive Processing to Harness and Implement Graphene Technology for Wear and Corrosion Protection

5a. CONTRACT NUMBER	5b. GRANT NUMBER	5c. PROGRAM ELEMENT NUMBER
		0605853N/2098
5d. PROJECT NUMBER	**5e. TASK NUMBER**	**5f. WORK UNIT NUMBER**
NRP-22-N275-A		

6. AUTHOR(S)

Ansell, Troy Y.

7. PERFORMING ORGANIZATION NAME(S) AND ADDRESS(ES)

Department of Mechanical and Aerospace Engineering, Naval Postgraduate School
Monterey, CA

8. PERFORMING ORGANIZATION REPORT NUMBER

NPS-MAE-22-003

9. SPONSORING/MONITORING AGENCY NAME(S) AND ADDRESS(ES)	10. SPONSOR/MONITOR'S ACRONYM(S)	11. SPONSOR/MONITOR'S REPORT NUMBER(S)
N9 - Warfare Systems		NPS-MAE-22-003; NRP-22-N275-A

12. DISTRIBUTION/AVAILABILITY STATEMENT

Distribution Statement A: Approved for public release. Distribution is unlimited.

13. SUPPLEMENTARY NOTES

14. ABSTRACT

Graphene is an amazing two dimensional material that has garnered much attention since it was first fabricated nearly 20 years ago. Since its discovery in 2006, scientists and engineers have attempted to find applications of graphene, both standalone and as a part of a composite material, to bring the nanomaterial to market. As of 2022, nearly 20 different products have come to market taking advantage of one or more of graphene's amazing properties, e.g., use as a flexible touch screen for smartphones because of the high electrical conductivity, stiffness, and optimal optical properties of graphene. This study focused on using graphene in both a polymer matrix composite and in an aluminum cold-sprayed coating. Graphene was added to a common polymer, polyethylene terephthalate glycol (PETG), to improve the hardness, wear resistance, and UV resistance of the polymer. The nanomaterial improved the hardness and wear resistance but experienced greater degradation when exposed to UV-B radiation at high temperature and humidity. Graphene was also added to Al powders, which were then cold sprayed onto an aluminum substrate. The graphene improved the hardness and adhesion strength of the coating but saw reduced wear resistance. Both effects were attributed to the interaction of the graphene with the Al "splats" in the coating.

15. SUBJECT TERMS

Graphene, Additive Manufacturing

16. SECURITY CLASSIFICATION OF:			17. LIMITATION OF ABSTRACT	18. NUMBER OF PAGES
a. REPORT	b. ABSTRACT	C. THIS PAGE		
U	U	U	UU	48

19a. NAME OF RESPONSIBLE PERSON	19b. PHONE NUMBER *(Include area code)*
Troy Y. Ansell	831-656-3033

STANDARD FORM 298 (REV. 5/2020)
Prescribed by ANSI Std. Z39.18

THIS PAGE INTENTIONALLY LEFT BLANK

NAVAL POSTGRADUATE SCHOOL
Monterey, California 93943-5000

Ann E. Rondeau
President

Scott Gartner
Provost

The report entitled "Using Additive Processing to Harness and Implement Graphene Technology for Wear and Corrosion Protection" was prepared for CMDR John Lucas, CAPT Holman Agard, and Mr. Bryant Kincaid of N9 – Warfare Systems and funded by the Naval Postgraduate School, Naval Research Program (PE 0605853N/2098).

Distribution Statement A: Approved for public release. Distribution is unlimited.

This report was prepared by:

_____
Dr. Troy Y. Ansell
Research Assistant Professor

Reviewed by:

_____
Brian Bingham, Chairman
Mechanical and Aerospace Engineering

Released by:

_____
Kevin B. Smith
Vice Provide for Research

THIS PAGE INTENTIONALLY LEFT BLANK

ABSTRACT

Graphene is an amazing two dimensional material that has garnered much attention since it was first fabricated nearly 20 years ago. Since its discovery in 2006, scientists and engineers have attempted to find applications of graphene, both standalone and as a part of a composite material, to bring the nanomaterial to market. As of 2022, nearly 20 different products have come to market taking advantage of one or more of graphene's amazing properties, e.g., use as a flexible touch screen for smartphones because of the high electrical conductivity, stiffness, and optimal optical properties of graphene. This study focused on using graphene in both a polymer matrix composite and in an aluminum cold-sprayed coating. Graphene was added to a common polymer, polyethylene terephthalate glycol (PETG), to improve the hardness, wear resistance, and UV resistance of the polymer. The nanomaterial improved the hardness and wear resistance but experienced greater degradation when exposed to UV-B radiation at high temperature and humidity. Graphene was also added to Al powders, which were then cold sprayed onto an aluminum substrate. The graphene improved the hardness and adhesion strength of the coating but saw reduced wear resistance. Both effects were attributed to the interaction of the graphene with the Al "splats" in the coating.

THIS PAGE INTENTIONALLY LEFT BLANK

TABLE OF CONTENTS

THIS PAGE INTENTIONALLY LEFT BLANK

LIST OF FIGURES

THIS PAGE INTENTIONALLY LEFT BLANK

LIST OF TABLES

THIS PAGE INTENTIONALLY LEFT BLANK

I. INTRODUCTION

A. BACKGROUND

Graphene was first intentionally isolated in 2004, an effort that resulted in the award of the Nobel Prize in Physics [1]. In the ensuing time, graphene has been studied for its extraordinary properties and ability to confer those properties onto other materials in a composite. Graphene has exhibited excellent mechanical and electrical properties, high thermal conductivity, and has a high degree of chemical inertness [2]. These amazing properties are due to the two-dimensional (2D) structure of graphene. The 2D structure of graphene endows it with a very high specific surface area, enabling more contact area for reinforcing a composite material or providing transfer of electrons or phonons [3], [4]. The high surface area can also be harnessed as a diffusion barrier, for example, for oxidizing or corrosive species. Despite the amazing properties exhibited by graphene, direct use of the nanomaterial in a naval application has yet to materialize. The time is ripe to attempt to harness this exciting material and implement it new technologies that can deliver anti-wear and anti-corrosive solutions to the Navy.

One set of applications of graphene that may prove beneficial is as a filler in composite materials, which can be used as a protective coating for metallic surfaces or as stand-alone components. Graphene may also contribute to improved wear resistance of the composite. This property may improve the life of coatings applied to many surfaces for different reasons, i.e., corrosion protection, wear protection, etc. Graphene has been shown to impart its excellent mechanical and functional properties in polymeric, metallic, and ceramic matrix composites. The “flat” structure of graphene also makes it suitable for material processing techniques that apply high pressure, such as cold gas dynamic spray (i.e., cold spray) that is beginning to be implemented in shipyards as a new repair technology. Cold spray is considered an additive manufacturing (AM) technique as it builds up a coating or freestanding part as a site of need. Another common AM technique, fused deposition modeling (FDM), could also be utilized to combined printable polymers with graphene to take advantage of the latter’s high wear resistance and high thermal and electrical conductivity.

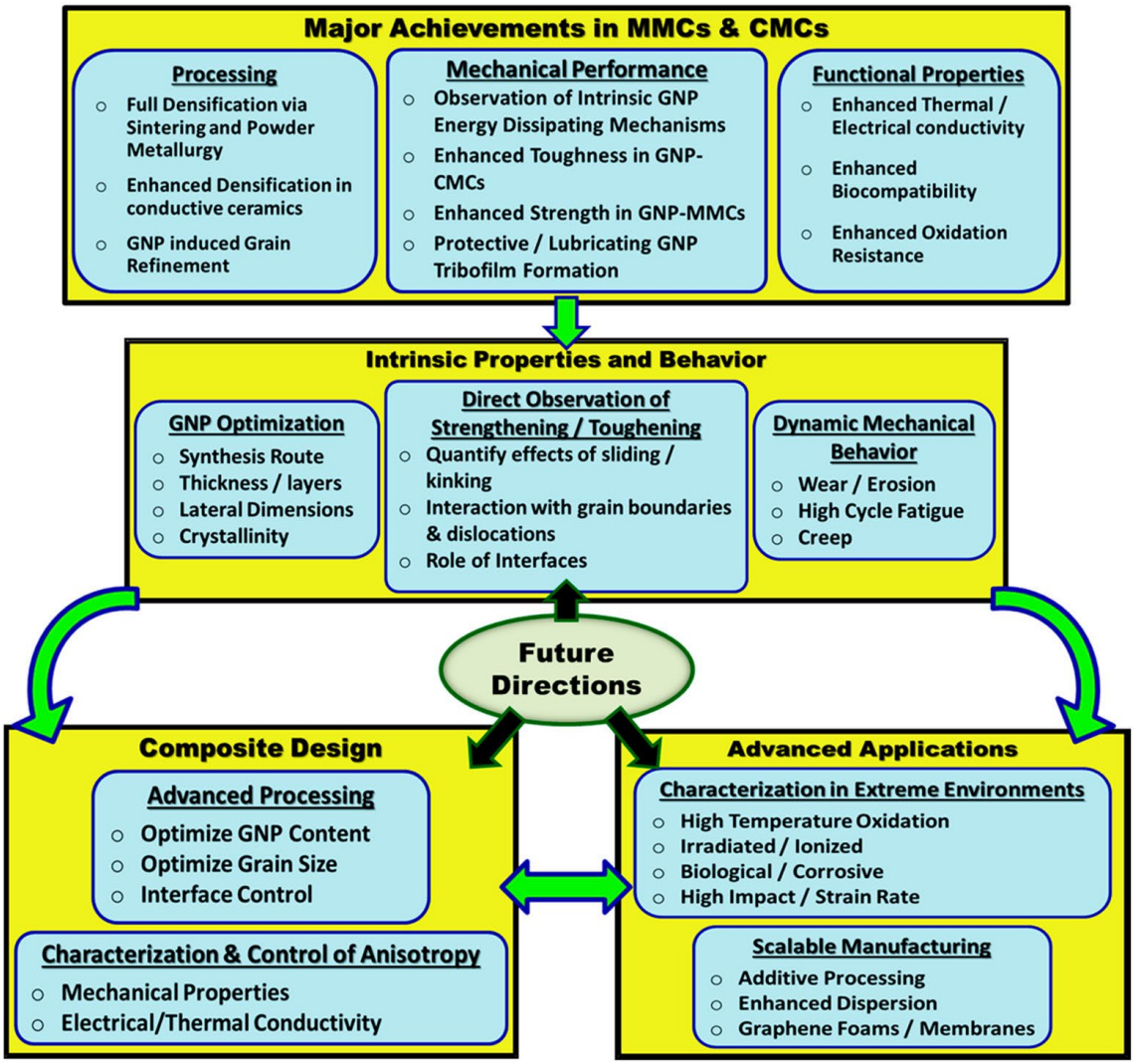

Figure 1. Current status of graphene in applications [4].

B. RESEARCH OBJECTIVES

The overall goal of this study was to incorporate graphene into conventional naval materials like aluminum or a printable polymer like polyethylene terephthalate glycol (PETG) to enhance their wear and corrosion resistance. It is the goal of this effort to provide analysis and quantifiable data to identify applications where graphene can be incorporated into naval uses by providing enhanced performance (reduction in maintenance, weight, life extension) at a cost benefit. Another goal was to investigate the role graphene and its derivatives could play in the environment, both negative and positive. Included in the latter is any possible *in vivo* effects of adding graphene to metal matrix and polymer matrix composites.

The rest of this report will be split into chapters. Chapter 2 will be a review of research on the environmental effects of graphene. This chapter will also briefly discuss the cost and benefits of adding graphene to composite materials although research in this is limited as will be seen. Chapters 3 and 4 will cover research conducted at NPS into adding graphene nanoplatelets (GNPs) to composite materials. Chapter 3 will show the experimental methods used in this research and chapter 4 will showcase the results.

THIS PAGE INTENTIONALLY LEFT BLANK

II. ASSESSMENT OF THE ENVIRONMENTAL IMPACTS AND COST BENEFIT OF GRAPHENE IN COMPOSITE MATERIALS

A. ASSESSMENT OF ENVIRONMENTAL AND HEALTH CONCERNS OF GRAPHENE

Owing to the amazing properties of graphene, the family of graphene nanoparticles (graphene, GNPs, carbon nanotubes, etc.) and its derivatives, graphene oxide and reduced graphene oxide, are growing in commercial importance. This comes with a growing concern of the impact to the environment these nanoparticles may have. Multiple pathways exist for these nanoparticles to enter waterways, the air, and soil. These pathways include applications of graphene nanoparticles as well as the fabrication of these nanoparticles. A major application of graphene is as an absorbent used to heavy metals and undesirable ions like ammonium from wastewater, drinking water, or in the desalination of seawater [5]. Mishra and Ramaprabhu investigated the use of functionalized graphene in a water filter to remove arsenic ions (both trivalent and pentavalent ions) and sodium ions from an aqueous solution [6]. This investigation and others have looked at the desalination of seawater using graphene and its derivatives [6]–[10]. Surwade et. al. found that a porous graphene sheet could reject nearly 100% of salt ions and some gases from water flowing through it [10].

Use as absorbents will likely be a major pathway for graphene to get into waterways and large bodies of water like the oceans. Graphene nanoparticles could also end up in soil through the production of graphene-based materials. Introduction into the soil would also provide another path for these materials to get into the water supply. In the soil itself, however, graphene could potentially affect its chemical composition and even the resident biota [11], [12]. Extensive research in the unintended introduction of graphene into the soil and water has been made to date. What is less understood are the effects graphene-based nanoparticles may have on the ecology of contaminated habitats and whether the effects are negative. One recent study suggested that graphene in low concentrations (~ 100 mg/kg) will cause an increase in bacterial activity for a short time before returning to previous levels but would have an adverse effect for high concentrations (>1000 mg/kg) [13]. Other studies on the cytotoxicity of graphene and its derivatives on bacteria showed that direct contact with graphene will inactivate (i.e., kill)

gram-positive and to a lesser extent, gram-negative bacteria [14]. It was speculated that the sharp edges of graphene led to lacerations in the outer cell walls and subsequent breakdown of the cellular interiors. Similar results were reported for fungus [15], algae [16], plants [17], and animals [18].

One final pathway for graphene to enter the environment is through the degradation of nanocomposites like polymer-based composites with a photodegradable polymer matrix [19]. Decomposition can occur in the polymer with exposure to sunlight or other UV source releasing graphene. This is a concern when considering the work in this report combines graphene with PETG that is not especially tolerant of UV exposure.

B. COSTS AND BENEFITS OF GRAPHENE-BASED COMPOSITES

Despite the amazing properties of graphene, CNTs, and even graphitic oxides, these materials have yet to be introduced to market. Part of the reason for this is the high cost of producing any of the graphene products. Depending on the quality of the graphene, the cost for one kg (~ 2.2 lbs) was $250 in 2011 but decreased by an order of magnitude down to $20/kg by 2015 [20]. This matches analysis presented by Smith and Rodrigues [21].

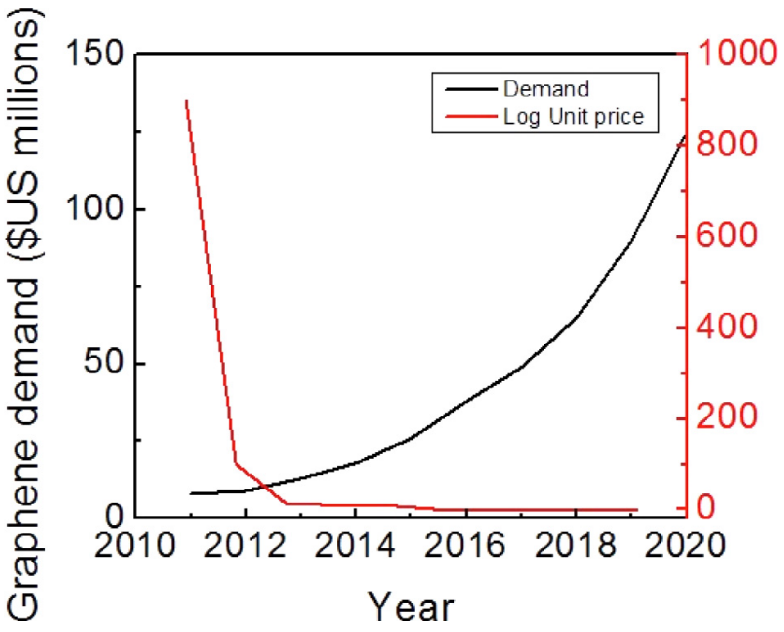

Figure 2. Demand and price of graphene (projected past 2015) after Lux Research Inc. and Graphenea [21].

Despite the high cost of graphene, CNTs, GO, and r-GO, increasing demand for these nanomaterials will further decrease the production costs and help with commercialization of these carbon polymorphs. Demand is increasing due to the many graphene-based products already available. Kong et. al. highlighted 17 different graphene based products available in market as of 2019 [20]. Some of these examples include graphene added to a silicon composite to be used as the anode in a Li-ion battery; as a standalone graphene film for use as a heat-sink in smartphones; and as a filler material in the rubber used for the shoes to improve the durability of the footwear. Graphene can be added to paints and coatings for improved corrosion resistance [20]. With the shrinking cost of graphene and the benefits already shown in numerous commercial products, the time to adopt graphene-based composite material for different naval applications may be close at hand. The following results will show small improvements in the mechanical properties of printed polymer-matrix composite parts and metallic matrix cold-sprayed (CS) coatings when a small amount of graphene nanoplatelets (GNPs) are added.

THIS PAGE INTENTIONALLY LEFT BLANK

III. EXPERIMENTAL METHODS

A. MATERIALS

The graphene nanoplatelets (GNPs) used throughout this study was purchased from XG sciences and had a thickness of 6 – 8 nm and an average width of 15 μm. Figure 2 shows a SEM image of a GNP. The GNP appears transparent with the underlying sample tape revealed. GNPs are thin enough for electrons to fully penetrate through. Clear PETG pellets were purchased from Felfil. The cold spray metal was an aluminum alloy purchased from Centerline Supersonic Spray Technologies. The aluminum and the metal matrix composite were sprayed onto Al-6061 substrates. This Al alloy is widely used for shipboard components.

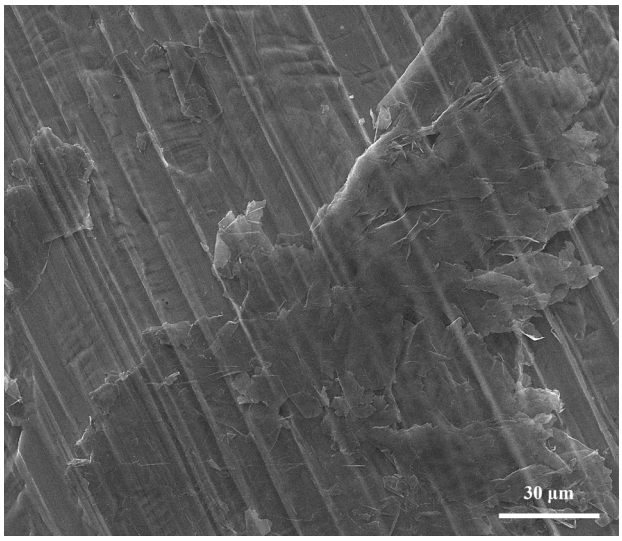

Figure 3. Image of a GNP taken in a SEM.

B. FABRICATION OF GRAPHENE INFUSED POLYMER COMPOSITES

Clear PETG pellets were mixed with no more than 1 vol% GNPs. PETG pellets and the mixture were placed, one at a time, in a Felfil filament extruder where the pellets are pulverized into a fine powder. The powder was then heated to a temperature of 210 ºC and filament extruded out at a speed of 5 RPM. Filament was placed in an oven set to 75 ºC afterward to dry. Filament was removed from the oven only for printing. Printing of the PETG with and without GNPs was done in a Lulzbot Mini 2 3D-printer. Polymer

parts were printed in simple square shapes 5 cm x 5 cm in width and length and a thickness of 3 mm.

After printing, the PETG and polymer composite samples were cut into two pieces of roughly the same size. One piece of each sample was exposed to increased ultraviolet (UV) radiation and temperature in a Q-Lab QUV accelerated weather tester. The exposure conditions were based on the ASTM standard G154 [22]. This entails exposing the samples to a UV irradiance of 1.55 W/m^2 and an elevated temperature of 60 ºC for eight hours, then a condensation cycle where the temperature is set to 50 ºC for four hours. This cycle of 8 hours UV/heat exposure followed by a 4-hour condensation step was repeated for three days (72 hours), equating to roughly one week of accelerated weathering.

C. FABRICATION OF GRAPHENE INFUSED METALLIC COMPOSITE COATINGS

Prior to spraying the MMC, the precursors were mixed using a high energy ball mill (HEBM). No more than 2 vol% graphene was mixed with the Al powders and placed in steel containers with stainless steel milling media and sealed. The sealed containers were then placed in a SPEX SamplePrep Mixer/Mill 8000D. HEBM is a process where particles undergo numerous collisions with stainless steel milling media. This leads to fracture, welding, and fusion of the particles [23]. Because the milling media (i.e., milling balls) are stainless steel, careful control of HEBM parameters including the ball-to-powder ratio is needed to prevent excessive deformation of the Al particles [24]. This is important for cold spray, and powder based AM processed, where particles need to be small and uniform in size and dimensions.

After mixing of the Al and Al-GNP composites, both are placed in an oven, set to 75 ºC, the night before spraying to remove any moisture. All samples were sprayed using a Centerline Supersonic Spray Technologies division (SST) Series P Spray Machine, with an X-Feeder, and a Series P Automatic Spray Gun. The surface of each substrate was roughened before spraying using an Eastwood Benchtop Blast Cabinet with aluminum oxide (Al_2O_3) blast media. Roughening the surface of the substrate increases the adhesion of the first layer of the coating. This increase is due to better mechanical interlocking

between the particles and the substrate surface. A smooth substrate causes more particles to bounce off until a thin layer of particles begins to build up.

Upon completion of spraying, samples underwent heat-treatment. Appropriate post-processing heat-treatment can improve the hardness and wear resistance of CS coatings due to densification, recrystallization, and nucleation of hard intermetallic precipitates [25], [26]. In this study, heat-treatment of both the Al and composite CS samples was done in an MTI OTF-1200X compact split tube furnace. To avoid contamination, samples were placed in a clean alumina crucible and placed in the furnace. Air was evacuated and replaced with argon gas (down to a pressure of 0.04 MPa) to avoid oxidation of the samples. The temperature was increased to 400 ºC during a 20-minute period. The samples were left at this temperature for one hour and then allowed to cool down to 150 ºC in the furnace before removal. Argon gas flowed during the entire heat-treatment.

D. SAMPLE CHARACTERIZATION

1. Materials Characterization

Some of the samples were mounted into an epoxy resin for further microscopic analysis. The epoxy used was either Struers ClaroCit, a fast-curing acrylic cold mounting resin, or Struers EpoFix slow-curing transparent cold mounting resin. Each mount was made according to the manufacturer's instructions. These sample mounts were ground flat and hand polished to expose details in the coatings by obtaining a mirror finish, free of large scratches. This analysis was done in both a Nikon Epiphot 200 optical microscope (with 2.5X, 10X, 20X, and 50X objective apertures) and a scanning electron microscope (SEM). The SEMs used in this study included a Thermo-Fisher Scientific (for the rest of this report, FEI) Inspect f50, a FEI Helios 5-UX, and a Zeiss Neon 40. Each SEM has differing parameters like objective aperture and voltage and current of the electron beam, but the typical working distance used across all SEMs is 5 mm.

2. Mechanical Characterization

A line of 15 micro-indents were applied to the surface of polished CS samples for Vicker's hardness measurement. These measurements were run at the HV 0.05 load and

conducted on a Struers DuraScan Vickers hardness tester. Micro-indents were applied to the cross-sectional area within the coating. Pores and scratches were avoided during this testing. Nano-indentation tests were conducted on the Al-GNP composites with an array of 50 nano-indentations on each cross-section using an Agilent G200 Nano-indenter. Hardness (at the nanoscale) and elastic modulus of the samples were calculated using the Oliver-Pharr method [27], [28].

Nano-indentation also allows for the determination of plasticity. Starting from an origin, testing begins by loading the sample with progressively higher loads until a preset maximum of 2mN is reached. The maximum load was held for three seconds and then slowly unloaded. Concurrently, a loading line that relates the load with the displacement of the indenter is generated. Loading lines that had a convex shape were removed as this is characteristic of indenter slipping during the testing. Loading lines with a concave shape were saved and the portion of the curve during unloading was used to calculate the elastic modulus and plasticity of the samples.

An Elcometer 510 Model T automatic adhesion tester was used to determine the adhesion strength of the CS coatings to the underlying substrate following the ASTM C633 standard [29]. Aluminum dollies with 10 mm diameter surface were glued to the coating surface using Master Bond EP15ND-2 high strength heat-curing epoxy. The epoxy, once applied, was cured according at a temperature between 300 – 350°C for 60-90 min. Once cured, the attached dollies were inserted into the adhesion tester. The applied pull rate on the dollies was 1.034 MPa/s (~150 psi/s).

Wear testing was performed on both polymer and polymer composite samples and Al CS samples. Each sample underwent at least three dry sliding ball-on-disk wear tests (an example seen in Figure 3). All wear tests were performed on a Nanovea T50 tribometer. The sample surface was worn down by rotation of 3 mm stainless steel 304 balls, at 100 RPMs, about a defined axis with a diameter of 6 mm for one hour. The wear balls were pushed down on the sample surface with a 3 N force. Wear debris was collected for further analysis. The depth of the encoder and coefficient of friction (COF) were recorded in real-time with a data collection rate of 20 data points/s.

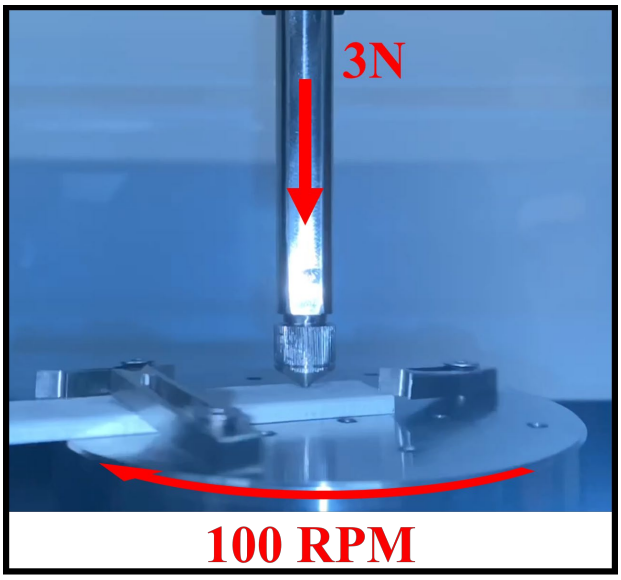

Figure 4. Still image taken from a video of a wear test being conducted.

THIS PAGE INTENTIONALLY LEFT BLANK

IV. RESULTS AND DISCUSSION

A. GRAPHENE INFUSED PETG

Completed filaments are shown in Figure 2 before and after sectioning. The individual layers can be seen in the clear PETG in Figures 2a and 2b. The outer layers (i.e., the "skin" indicated by the red solid arrow) measured approximately 1.4 mm in diameter while the inner layers (indicated by the orange dashed arrow) measured about 1.25 mm. The clear PETG had well defined layers, this is in comparison to the PETG-GNP composite seen in Fig. 2c. The composite layer dimensions were like those of the clear PETG polymer. The big difference is the color, the small addition of GNPs had the big effect of changing it from clear to black. QUV testing was stopped after 72 hours as samples were already beginning to deform due to the combined temperature and UV exposure. Wear testing is hard to perform on curved surfaces.

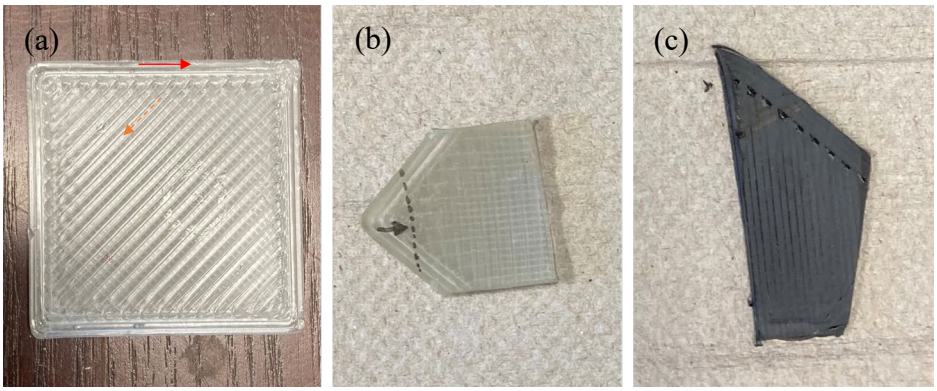

Figure 5. Images of PETG taken after printing. (a) Clear PETG before sectioning; (b) clear PETG after sectioning; and (c) PETG-GNP after sectioning.

Wear testing was performed on both the as-printed and QUV tested PETG and PETG-GNP samples. Although mass loss in the samples and the mass of debris collected during wear testing can be used to estimate the volume of the wear track. It is often difficult to gather wear debris or accurately measure mass changes in the bulk sample when debris collected is small (on the order of mg by mass). This is especially true for the PETG printed in this work, due to its elastic character. An alternative is optical profilometry that can image the wear tracks and calculate the surface height of the wear track at various surface locations. This technique was performed on these samples after

undergoing wear testing. Examples of results are shown in Figure 3 for PETG, the height or elevation map of the as-printed sample (Fig. 3a) and a line profile (Fig. 3c); and the same for a PETG sample after QUV testing in Figures 3b and d. The line profiles are generated by defining a line in the map (look for a line with arrows in Figs. 3a and b).

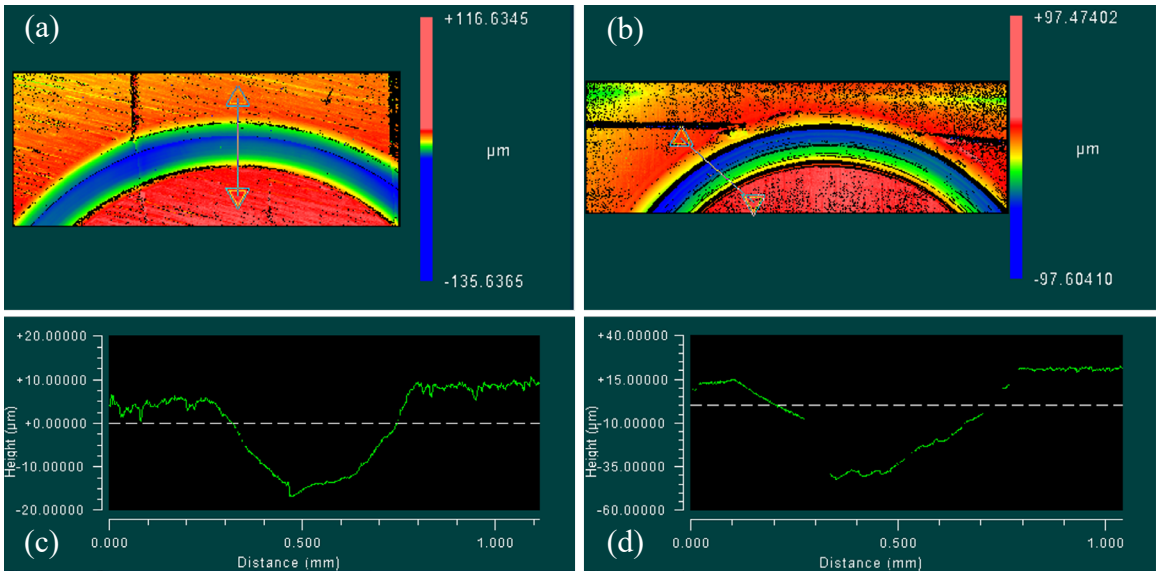

Figure 6. Examples of optical profilometry maps and line profiles. The as-printed PETG map, (a), and the QUV PETG map in (b). The as-printed PETG line profile, (c), and the QUV PETG line profile in (d).

Figure 4 shows plots of wear test data performed on the printed plastics both before and after QUV exposure. The data is of the wear width (Fig. 4a), depth (Fig. 4b), and coefficient of friction (COF in Fig. 4c). Wear track width and depth is lower for the PETG-GNP sample as compared to the PETG before for the as-printed samples. QUV testing causes a reversal. The wear tracks on the QUV tested polymer composite was both wider and deeper than the QUV PETG sample. Of note is the narrow variance seen in the GNP samples, even in the QUV tested composite. Assuming the surface roughness is similar between samples being compared, a higher COF means a lower resistance to wear. The results of Figure 4c suggests that the as-printed PETG-GNP sample exhibited similar wear resistance compared to the pure PETG. For the samples exposed to UV and increased temperature, the difference in COF was larger but the variance in the composite data suggests that again, there is no statistical difference in wear resistance based on the COF.

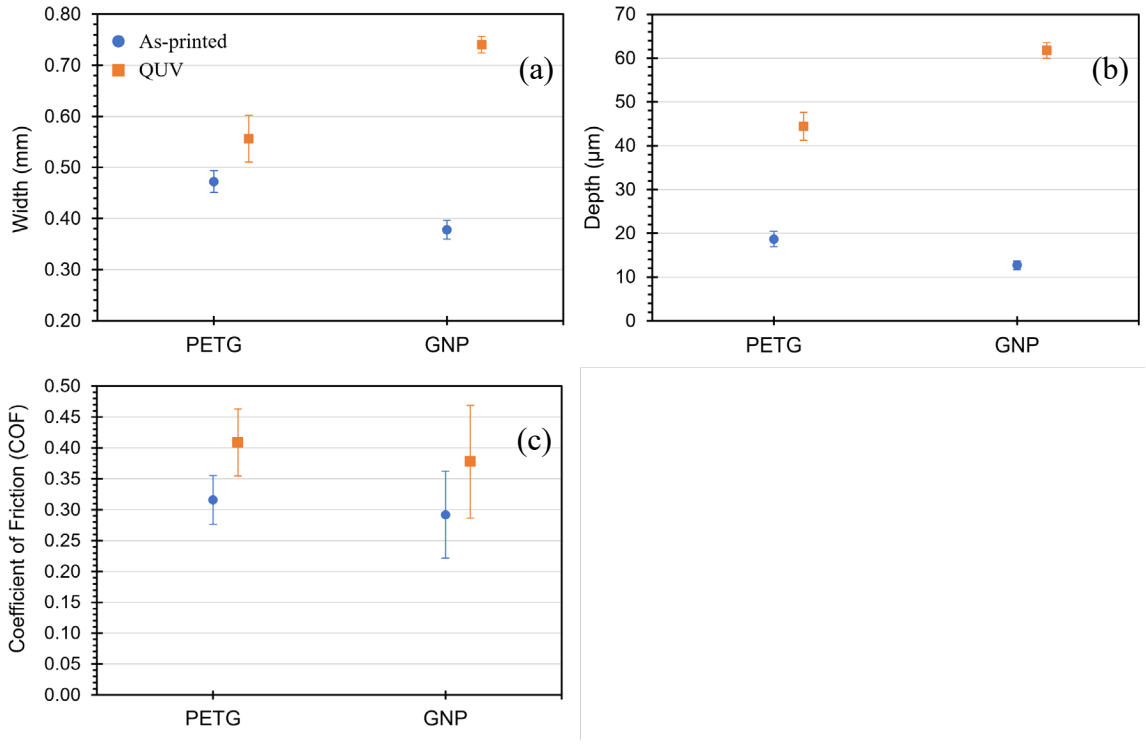

Figure 7. COF of both as-printed and QUV tested PETG and PETG-GNP samples

B. GRAPHENE INFUSED ALUMINUM COLD SPRAYED COATINGS

1. General Coating Properties

An important parameter when measuring the performance of a cold sprayed coating is the coating thickness. The mean thickness and percent porosity are listed in Table 1 with their standard deviations. The coating thickness of Al and the Al-GNP CS coatings were measured in the SEM as seen in Figure 4. The composite coating, sprayed onto the same alloy with the same parameters as the Al coating, deposited a thinner layer. Using ImageJ to analyze the SEM images revealed a measurable decrease in the number of pores, i.e., the Al-GNP coating was denser than the Al coating.

Table 1. Thickness (t), mean t, and standard deviation of the coating thickness (σ_t) of the Al and composite coating. Coating porosity is included with its standard deviation (σ_p).

Composition	t [µm]	Mean t [µm]	σ_t [µm]	Porosity [%]	σ_p [%]
Al	462-694	561	47.4	5.2	3.0
Al-GNP	191-347	279	33.2	2.9	1.4

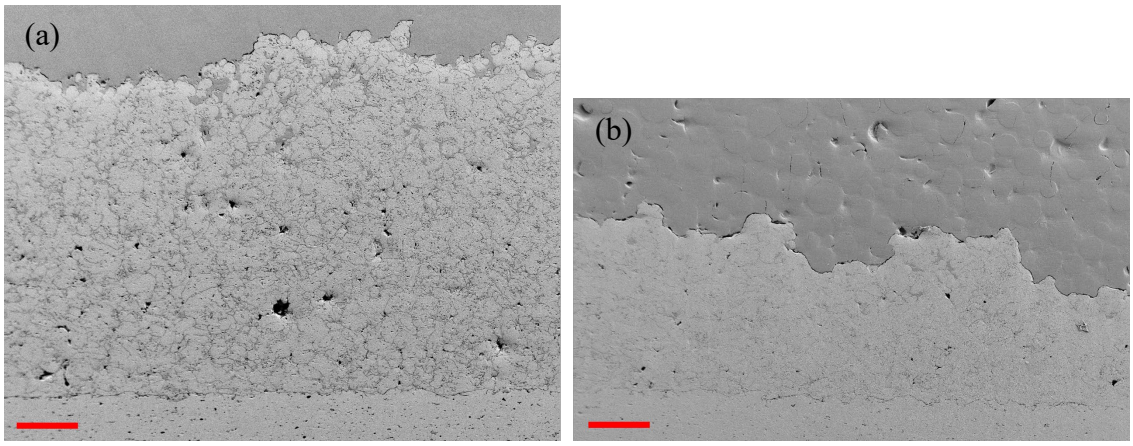

Figure 8. SEM images of (a) the pure Al coating and (b) the Al-GNP coatings.

2. Mechanical Properties

A materials hardness gives a measure of its ability to resist plastic deformation. Hardness measurements give a number based on the method and its related scale thus hardness is a comparative measurement and not a fundamental materials property [ref]. Despite this limitation, the measurement is a simple technique to compare the strength of of materials. For the results of micro-indentation hardness tests done on CS Al and Al-GNP coatings are shown in Fig. 5a. The composite coating experienced a significant increase in hardness with 74.7% increase over the Al coating. Pinning of GNPs between the Al splats during heat treatment.

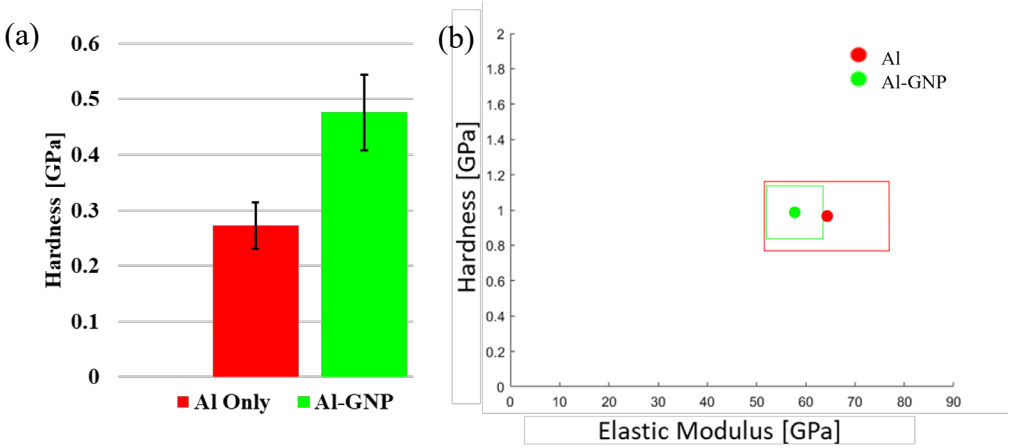

Figure 9. Results from (a) Vickers micro-indentation and (b) nano-indentation hardness measurements.

Figure 5b shows the results from nano-indentation hardness tests, which are used to calculate small-scale hardness and elastic modulus. Because of the large number of indents made relatively rapidly, this type of measurement gives a better statistical average hardness value of the matrix material. The red dot represents the mean hardness of 50 indents applied to the Al coating, while the green dot is the mean of the Al-GNP coating. Around each dot is a like colored bow which represents one standard deviation for that sample in terms of hardness (y-axis) and elastic modulus (x-axis). Outlier indentations e.g., indents that resulted in low hardness and large elastic modulus, were removed. This was justified as the indents fell on a pore in the coating. Figure 5b shows that the box for Al-GNP coating was smaller than for the Al coating. The Al-GNP coating has about the same hardness as the pure Al coating but a 10% decrease in elastic modulus.

Load and displacement tests for each nanoindentation were analyzed and plotted in Figure 6 for both sets of samples. The red line represents the median test curve for that sample. Tests on the Al-GNP coating were again more precise compared to the Al coating. Using the unloading curves, plasticity was calculated from the ratio of maximum displacement to the displacement remaining after the load is completely removed. This calculation was performed for each nano-indentation and the averages were recorded. The Al-GNP coating had about the same plasticity as the pure Al.

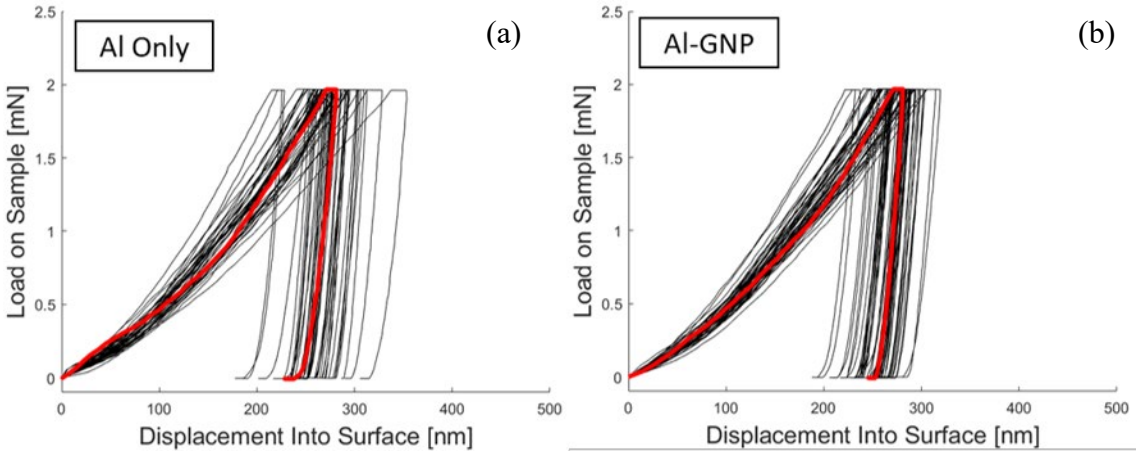

Figure 10. Load and displacement curves generated for (a) Al and (b) Al-GNP CS samples.

3. Coating Adhesion

The values for the maximum adhesion stress were averaged for each sample. Three modes of failure were observed during adhesion testing: failure between the coating and the substrate (i.e., delamination), failure within the coating, or failure between the high-strength epoxy and the dolly. Examples of each of these failure modes are seen in Figure 9. All five adhesion tests performed on the pure Al coating saw delamination failure as shown in Fig. 9a and 9b. This mode of adhesive failure occurred between the coating and substrate due to pulling of the surrounding coating instead of brittle-like fracturing of the coating under the dolly. This demonstrates the pure Al coating exhibits high cohesive strength within the coating layer. Adhesion tests conducted on the Al-GNP samples experienced adhesive failure as shown in Fig. 9c. These results likely experienced a mixture of failure modes between failure of the epoxy and failure within the coating. The mean adhesion strength of the Al-GNP coatings was slightly higher, at 12.5 MPa ± 1.40 MPa, as compared to the Al coating with an average adhesion strength of 12.0 MPa ± 1.17 MPa. The adhesion results suggest a slight improvement in the overall strength of the composite coating, but intra-coating cohesion appeared to be higher in the more porous pure Al coating. More testing will need to be done to resolve this discrepancy.

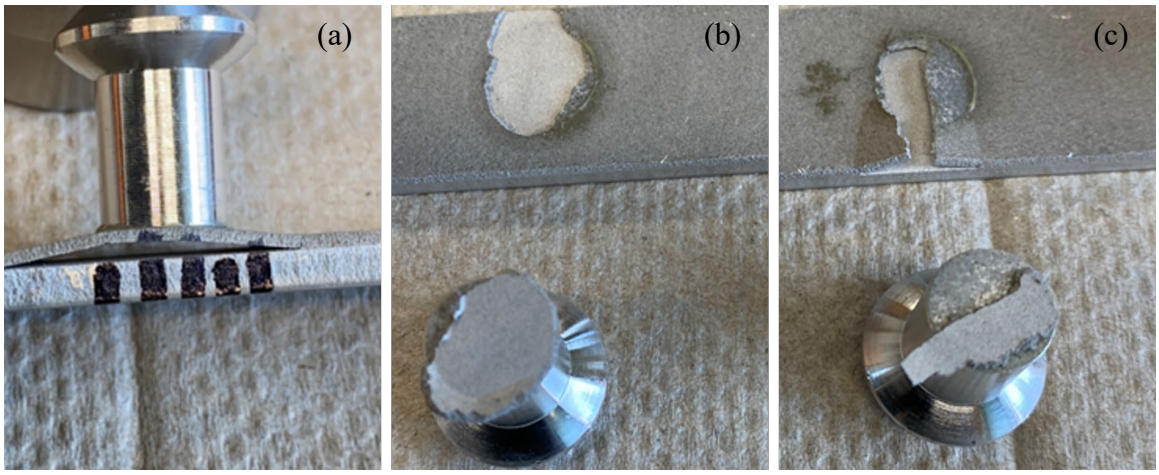

Figure 11. Images of samples after adhesion testing. The three types of failure shown here include: (a) adhesive failure with peeling, i.e., coating delamination; (b) adhesive failure; and (c) partial adhesive failure.

4. Wear Properties

Mass loss and COF of the two coatings after wear testing are presented in Figure 11. The amount of mass lost (Fig. 11a) from a surface due to wear is inversely proportional to a surface material's wear resistance. If the counter surface causing wear were the same for two surfaces being compared, than greater mass loss of one would suggest a greater amount of mechanical exfoliation and so lower wear resistance. The Al coating, while undergoing wear testing, experienced the lower amount of mass loss. Conversely, the Al-GNP coating experienced a greater amount of mass loss during wear testing suggesting lower wear resistance compared to the Al coating.

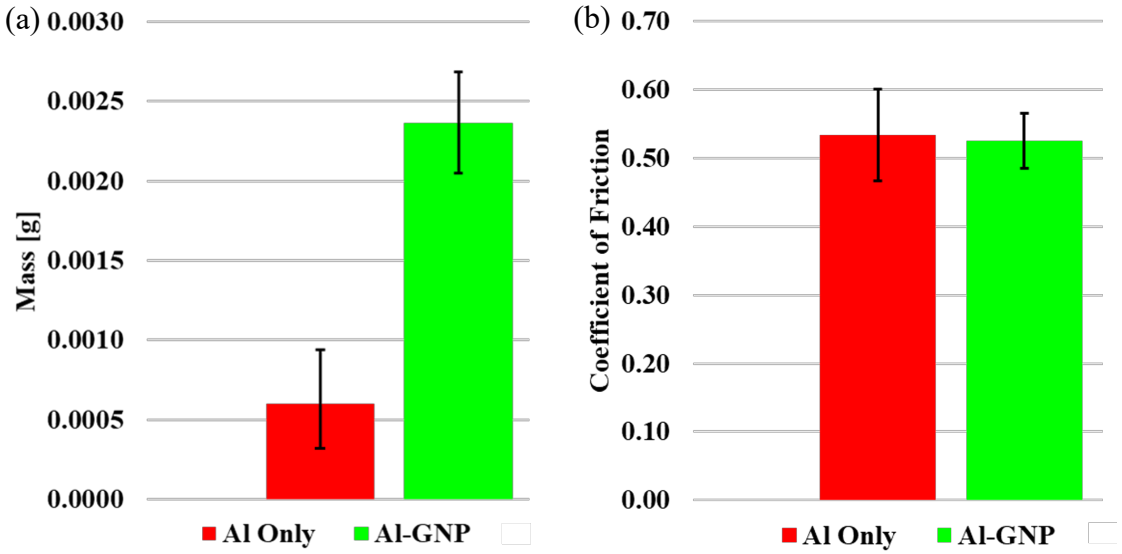

Figure 12. Results of wear testing on Al cold-sprayed coatings. Mass loss in (a) for both samples and COF in (b).

The COF (Fig. 11b) was recorded in real-time and the mean value with standard deviation plotted. It reveals somewhat contradictory evidence for wear resistance. If the wear resistance was lower for the Al-GNP coating, the COF of Al-GNP should be higher than for Al, which is not the case here. Another measure of wear resistance is the wear rate. A higher wear rate means less resistance to wear. The wear rate is calculated by taking the volume of material lost divided by the load times the total dry sliding distance (i.e., the total distance traveled by the wear balls). For all wear tests, the total dry sliding distance was 113.1 m and the load was 3 N. The volume lost is determined by dividing

the mass lost by the material density; for Al, the density is 2.66 g/cm^3 while GNPs are 2.52 g/cm^3. Because the cold spray layer is less than 100% dense, the nominal density is multiplied by unity less the porosity to reach a more realistic density. The calculated wear rate for the Al coating was 0.701×10^{-3} mm^3/Nm while for the Al-GNP coating, 2.741×10^{-3} mm^3/Nm. The composite coating had a nearly 4X higher wear rate!

C. DISCUSSION

1. PETG-GNP

Printed PETG saw slight improvement in wear resistance with the addition of a small amount of GNPs seen through a lower COF, narrower wear width, and shallower wear depth (Fig. 7). This was reversed after exposure to UV/heat/humidity. The dramatic decrease in wear resistance seen in the PETG-GNP composites could be explained as a combination of the embrittlement of the PETG matrix, which was also seen with the plain PETG sample, and the "release" of the GNPs during wear testing. Work on the accelerated aging, i.e., UV exposure, of PETG printed polymers was performed by Amza et al. [30], [31]. They found that UV exposure caused a degradation in mechanical properties of the printed PETG. Although tensile strength was looked at, there is a correlation between strength, hardness, and wear resistance. In this case, with GNPs embedded in PETG, the aging effects are increased, especially during wear. The individual GNPs were unlikely fully connected to the surrounding polymer chains within the PETG. After exposure to UV, heat, and humidity, the GNPs now loosely connecting PETG grains come out of the bulk material taking the PETG grain with it. An example of this can be seen Figure 13. In Figure 13c and 13d, a PETG grain has come out of the bulk after wear testing. At one end, a separate piece of debris sits. It was identified as a GNP due to its size and aspect ratio. Numerous SEM images were taken of both the PETG and PETG-GNP samples both QUV-tested and not. A general theme was the smooth nature of the samples except for the QUV-tested PETG-GNP, which exhibited a roughened surface.

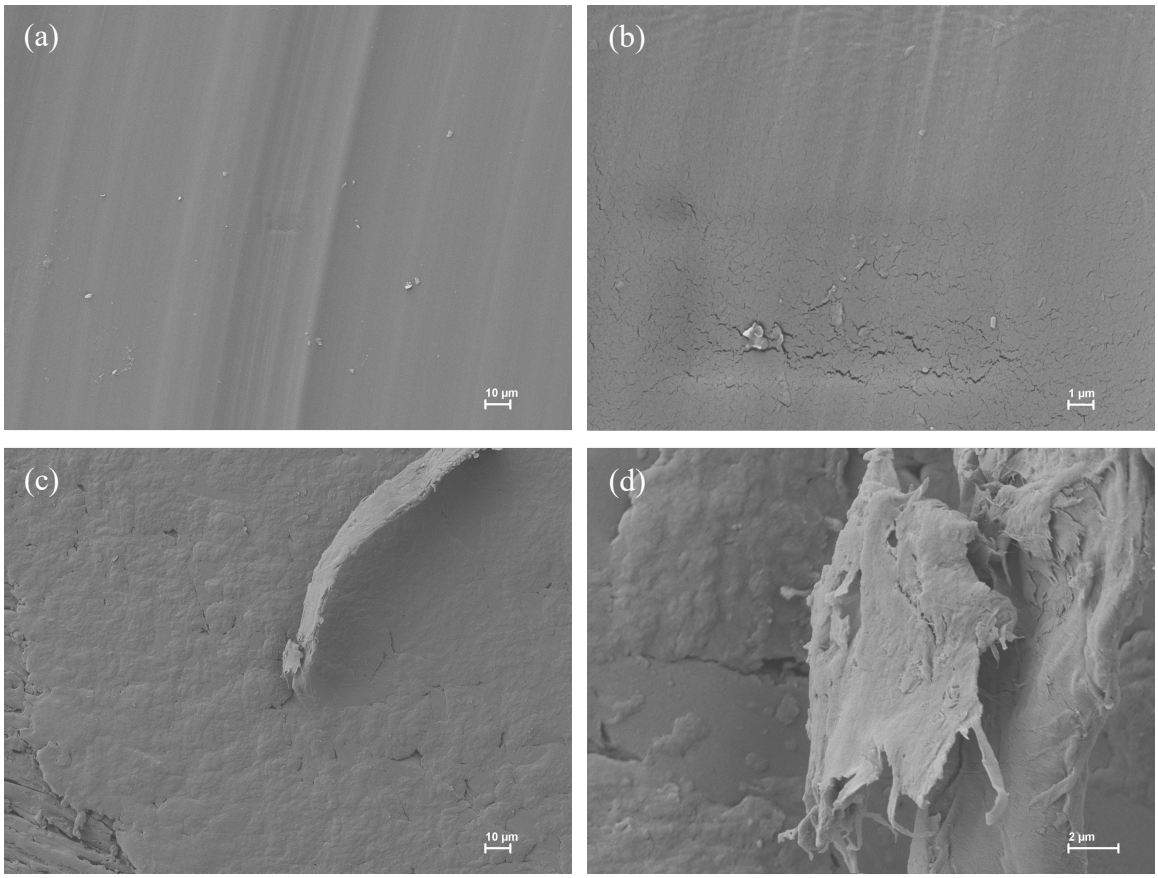

Figure 13. SEM images of QUV-tested PETG at (a) low magnification and (b) high magnification and QUV-tested PETG-GNP at (c) low magnification and (d) high magnification.

2. Al-GNP

GNPs are formed of individual graphene layers. Each graphene platelet exhibits high in-plane strength, meaning the possible force that can be applied parallel to the plane is high. The strength of a GNP normal to the sheets is weak in comparison as it relies only on weak van der Waals forces. This fact: however, allows the graphene sheets to easily slip past one another during a shear event. This in turn can lead to dispersion of the individual graphene sheets across a composite material. Unfortunately, when added to a composite, this high strength is not fully transferred to the matrix. Further, the orientation of the individual platelets will affect the amount of reinforcing that occurs. Wider dispersion and higher concentration of graphene is therefore a key requirement when reinforcing a material in composite.

Because of the milling process, the GNPs may attach to individual Al particles but will not fully integrate into the particles. After spraying, therefore, the GNPs or individual graphene sheets will reside in the sprayed particle (also referred to as a splat because of the shape after impact) boundary layer, the splat boundaries as shown in Figure 14. Assuming adequate GNP dispersion, the high contact area between a splat and a GNP will lead to effective load transfer between the splat and splat boundary and visa versa. This is one of the key strengthening mechanisms found in composite materials. Graphene sheets sliding past one another and/or compression of the GNPs both could absorb energy and prevent microcracks within the splat boundary from growing and propagating.

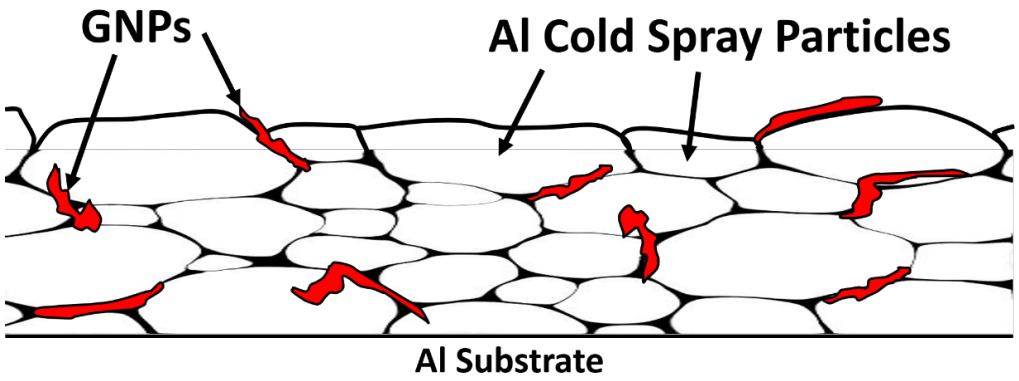

Figure 14. Schematic of GNPs among the Al CS splats .

SEM images of adhesion surfaces of the Al-GNP coating are shown in Figure 15. Figures 15a and 15b is a cross-section taken of the adhesion fracture surface. This sample was prepared to look at the interaction between the GNPs and the splats after the tensile forces experienced by the sample during adhesion testing. In these images and others taken of the adhesion cross-section, GNPs were often found to “bridge” splats. What is expected from this is an increase in adhesion strength of the overall sample. A slight increase in adhesion strength was observed in the composite coating over the Al coating. Figures 15c and 15d shows top-down images of the fracture surface after adhesion testing. GNPs are shown again between splats. Frictional forces between the GNPs and splats also assist in strengthen of the coating.

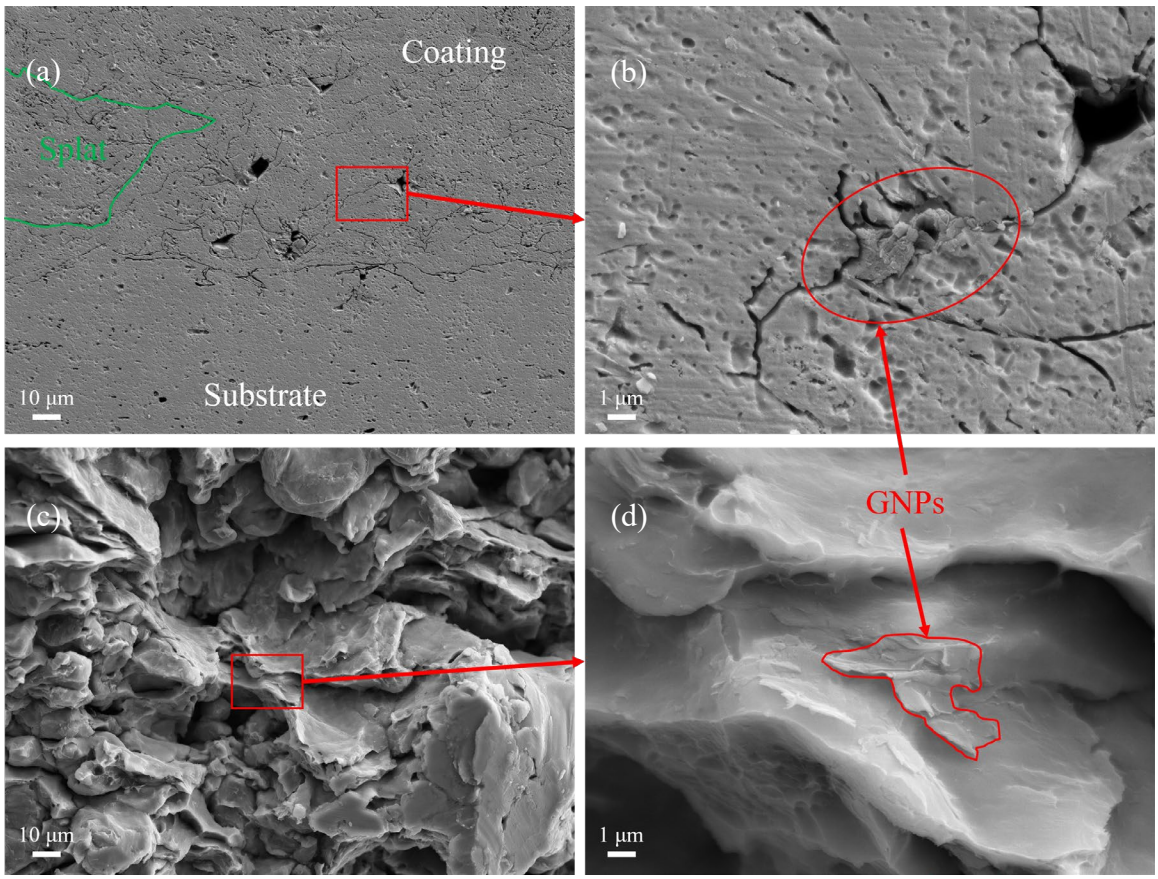

Figure 15. SEM images of the adhesion cross-section of Al-GNP at (a) low and (b) high magnification and the adhesion fracture surface of Al-GNP at (c) low and (d) high magnification.

Table 2 summarize the differences in testing results of the Al and Al-GNP coatings. The composite coating showed decreased porosity after heat treatment; however, the cold spraying resulted in a thinner coating as compared to the Al coating. The cause was likely due to clogging of the cold spray nozzle. When spraying with the composite powders, the nozzle would clog due to GNPs depositing on the interior surface of the nozzle. The micro-indentation hardness of the Al-GNP was 75% higher than the pure Al coating, while the difference in nano-hardness and elastic modulus were negligible. The Al-GNP also had smaller variance in nanoindentation tests. Plasticity was indistinguishable for the two coatings. The micro-indenter creates a larger indent with a larger load of the surface increasing the chances of indenting splats with attached GNPs. The chances of this happening with the nano-indenter were low in comparison. The nano-

indenter hit a larger proportion of bare matrix material measuring values closer to that of the Al.

The wear loss in the GNP sample was 300% higher than the loss found in the Al coating. Further the wear depth was 50% deeper. Despite the improvements in the hardness, the decrease in wear resistance of the composite coating is also due to the GNPs presence. Because of the bridging of splats by the GNPs, when a splat comes lose from the bulk, it brings along a GNP. So, instead of lubricating the surface as graphene normally does in cases of frictional relief, the splat/GNP combination contributes to wear of the surface.

Table 2. List of Results of Al and Al-GNP.

Sample	Coating Thickness [µm]	Porosity [%]	Micro-Hardness [GPa]	Nano-Hardness [GPa]	Elastic Modulus [GPa]
Al	561 ± 48	5.2 ± 3.0	0.27 ± 0.04	0.97 ± 0.20	64.4 ± 12.8
Al-GNP	279 ± 33	**2.9 ± 1.4**	**0.48 ± 0.07**	0.99 ± 0.15	57.8 ± 5.79
Sample	**Plasticity [%]**	**Adhesion Strength [MPa]**	**Mass Loss [mg]**	**Wear Depth [µm]**	**COF**
Al	89.8 ± 2.4	12.0 ± 1.2	0.6 ± 0.3	8.52 ± 1.78	0.53 ± 0.07
Al-GNP	89.3 ± 1.7	12.5 ± 1.4	2.4 ± 0.3	13.5 ± 2.33	0.53 ± 0.04

THIS PAGE INTENTIONALLY LEFT BLANK

V. CONCLUSION

Graphene nanoplatelets (GNPs) were added (up to 1 vol%) to PETG FDM printer filament, which was printed. The small addition of GNPs greatly reduced the transparency of the PETG, which was clear as received. Some of the samples were then exposed to UV-B radiation at higher temperatures and humidity to accelerate aging of the polymer. The polymer microstructure was examined, and samples were wear-tested. The composite polymers exhibited higher wear resistance before accelerated ageing, but the trend was reversed with a dramatic decrease in wear resistance of the composite polymer. GNPs were also added (this time at 2 vol%) to Al powder specially processed for cold spraying. These powders were sprayed onto Al-6061 substrate and the microstructure and mechanical properties were studied. The results were mixed as the micro-hardness and adhesion strength of the composite coating was slightly higher than the pure Al coating, but the wear resistance suffered. Both effects were attributed to the GNPs and their interaction with the Al splats.

Despite these mixed results, the amount of GNPs was low and unlike carbon nanotubes (CNTs), GNPs are easier to disperse during mixing. So, a higher concentration of GNPs should be possible and may lead to greater improvements in mechanical properties. Use of graphene-based nanoparticles are increasing in application and with a dramatic decrease in cost, applications taking advantage of the nanoparticles are increase substantially soon. Careful considerations: however, should be made when using graphene as large quantities unintentionally added to the environment including our own bodies may lead to unintended negative effects.

THIS PAGE INTENTIONALLY LEFT BLANK

LIST OF REFERENCES

[1] K. S. Novoselov *et al.*, "Electric Field Effect in Atomically Thin Carbon Films," *Science*, vol. 306, no. 5696, pp. 666–669, Oct. 2004, doi: 10.1126/science.1102896.

[2] D. R. Cooper *et al.*, "Experimental Review of Graphene," *ISRN Condensed Matter Physics*, vol. 2012, p. 501686, Apr. 2012, doi: 10.5402/2012/501686.

[3] C. Soldano, A. Mahmood, and E. Dujardin, "Production, properties and potential of graphene," *Carbon*, vol. 48, no. 8, pp. 2127–2150, 2010.

[4] A. Nieto, A. Bisht, D. Lahiri, C. Zhang, and A. Agarwal, "Graphene reinforced metal and ceramic matrix composites: a review," *International Materials Reviews*, vol. 62, no. 5, pp. 241–302, 2017.

[5] J. Zhao, Z. Wang, J. C. White, and B. Xing, "Graphene in the aquatic environment: adsorption, dispersion, toxicity and transformation," *Environmental science & technology*, vol. 48, no. 17, pp. 9995–10009, 2014.

[6] A. K. Mishra and S. Ramaprabhu, "Functionalized graphene sheets for arsenic removal and desalination of sea water," *Desalination*, vol. 282, pp. 39–45, 2011.

[7] D. Cohen-Tanugi and J. C. Grossman, "Water Desalination across Nanoporous Graphene," *Nano Lett.*, vol. 12, no. 7, pp. 3602–3608, Jul. 2012, doi: 10.1021/nl3012853.

[8] M. Hu and B. Mi, "Enabling Graphene Oxide Nanosheets as Water Separation Membranes," *Environ. Sci. Technol.*, vol. 47, no. 8, pp. 3715–3723, Apr. 2013, doi: 10.1021/es400571g.

[9] D. Konatham, J. Yu, T. A. Ho, and A. Striolo, "Simulation Insights for Graphene-Based Water Desalination Membranes," *Langmuir*, vol. 29, no. 38, pp. 11884–11897, Sep. 2013, doi: 10.1021/la4018695.

[10] S. P. Surwade *et al.*, "Water desalination using nanoporous single-layer graphene," *Nature Nanotechnology*, vol. 10, no. 5, pp. 459–464, May 2015, doi: 10.1038/nnano.2015.37.

[11] A. Baysal, H. Saygin, and G. Ustabasi, "Risks of graphene nanomaterial contamination in the soil: evaluation of major ions," *Environmental Monitoring and Assessment*, vol. 192, no. 10, pp. 1–17, 2020.

[12] H. Chung *et al.*, "Effects of graphene oxides on soil enzyme activity and microbial biomass," *Science of The Total Environment*, vol. 514, pp. 307–313, May 2015, doi: 10.1016/j.scitotenv.2015.01.077.

[13] W. Ren, G. Ren, Y. Teng, Z. Li, and L. Li, "Time-dependent effect of graphene on the structure, abundance, and function of the soil bacterial community," *Journal of Hazardous Materials*, vol. 297, pp. 286–294, 2015.

[14] O. Akhavan and E. Ghaderi, "Toxicity of Graphene and Graphene Oxide Nanowalls Against Bacteria," *ACS Nano*, vol. 4, no. 10, pp. 5731–5736, Oct. 2010, doi: 10.1021/nn101390x.

[15] M. Sawangphruk, P. Srimuk, P. Chiochan, T. Sangsri, and P. Siwayaprahm, "Synthesis and antifungal activity of reduced graphene oxide nanosheets," *Carbon*, vol. 50, no. 14, pp. 5156–5161, 2012.

[16] S. Du *et al.*, "Reduced graphene oxide induces cytotoxicity and inhibits photosynthetic performance of the green alga Scenedesmus obliquus," *Chemosphere*, vol. 164, pp. 499–507, 2016.
[17] P. Zhang *et al.*, "Toxic effects of graphene on the growth and nutritional levels of wheat (Triticum aestivum L.): short-and long-term exposure studies," *Journal of hazardous materials*, vol. 317, pp. 543–551, 2016.
[18] X. T. Liu *et al.*, "Toxicity of multi-walled carbon nanotubes, graphene oxide, and reduced graphene oxide to zebrafish embryos," *Biomedical and Environmental Sciences*, vol. 27, no. 9, pp. 676–683, 2014.
[19] C. Bernard, T. Nguyen, B. Pellegrin, R. Holbrook, M. Zhao, and J. Chin, "Fate of graphene in polymer nanocomposite exposed to UV radiation," 2011, vol. 304, no. 1, p. 012063.
[20] W. Kong *et al.*, "Path towards graphene commercialization from lab to market," *Nature nanotechnology*, vol. 14, no. 10, pp. 927–938, 2019.
[21] S. C. Smith and D. F. Rodrigues, "Carbon-based nanomaterials for removal of chemical and biological contaminants from water: a review of mechanisms and applications," *Carbon*, vol. 91, pp. 122–143, 2015.
[22] "Standard Practice for Operating Fluorescent Light Apparatus for UV Exposure of Nonmetallic Materials," ASTM International, West Conshohocken, PA, Standard ASTM G154-06.
[23] P. S. Gilman and J. S. Benjamin, "Mechanical alloying," *Annu. Rev. Mater. Sci.*, vol. 13, no. 1, pp. 279–300, Aug. 1983, doi: 10.1146/annurev.ms.13.080183.001431.
[24] T. Y. Ansell, T. Hanneman, A. Gonzalez-Perez, C. Park, and A. Nieto, "Effect of high energy ball milling on spherical metallic powder particulates for additive manufacturing," *Particulate Science and Technology*, vol. 39, no. 8, pp. 981–989, Nov. 2021, doi: 10.1080/02726351.2021.1876192.
[25] S. B. Pitchuka *et al.*, "Dry sliding wear behavior of cold sprayed aluminum amorphous/nanocrystalline alloy coatings," *Surface and Coatings Technology*, vol. 238, pp. 118–125, 2014.
[26] S. B. Pitchuka, D. Lahiri, G. Sundararajan, and A. Agarwal, "Scratch-induced deformation behavior of cold-sprayed aluminum amorphous/nanocrystalline coatings at multiple load scales," *Journal of thermal spray technology*, vol. 23, no. 3, pp. 502–513, 2014.
[27] W. C. Oliver and G. M. Pharr, "An improved technique for determining hardness and elastic modulus using load and displacement sensing indentation experiments," *J. Mater. Res.*, vol. 7, no. 6, pp. 1564–1583, Jun. 1992, doi: 10.1557/JMR.1992.1564.
[28] W. C. Oliver and G. M. Pharr, "Measurement of hardness and elastic modulus by instrumented indentation: Advances in understanding and refinements to methodology," *J. Mater. Res.*, vol. 19, no. 1, pp. 3–20, Jan. 2004, doi: 10.1557/jmr.2004.19.1.3.
[29] "Standard Test Method for Adhesion or Cohesion Strength of Thermal Spray Coatings," ASTM International, West Conshohocken, PA, ASTM C633-13, 2013.
[30] C. G. Amza, A. Zapciu, F. Baciu, M. I. Vasile, and A. I. Nicoara, "Accelerated Aging Effect on Mechanical Properties of Common 3D-Printing Polymers," *Polymers*, vol. 13, no. 23, p. 4132, 2021.

[31] C. G. Amza, A. Zapciu, F. Baciu, M. I. Vasile, and D. Popescu, “Aging of 3D printed polymers under sterilizing UV-C radiation,” *Polymers*, vol. 13, no. 24, p. 4467, 2021.

THIS PAGE INTENTIONALLY LEFT BLANK

INITIAL DISTRIBUTION LIST

1. Defense Technical Information Center
   Ft. Belvoir, Virginia

2. Dudley Knox Library
   Naval Postgraduate School
   Monterey, California

3. Research Sponsored Programs Office, Code 41
   Naval Postgraduate School
   Monterey, CA 93943